THE JOURNAL OF PHYSICAL CHEMISTRY C
A JOURNAL OF THE AMERICAN CHEMICAL SOCIETY

pubs.acs.org/JPCC

Article

Understanding the Effect of Symmetry Breaking on Plasmon Coupling from TDDFT

Fahri Alkan* and Christine M. Aikens*

Cite This: *J. Phys. Chem. C* 2021, 125, 12198−12206

Read Online

ACCESS | Metrics & More | Article Recommendations | Supporting Information

ABSTRACT: We perform a time-dependent density functional theory (TDDFT) investigation for the optical properties of nanorod assemblies for different sizes (Ag_{10}, Ag_{59}, and Ag_{139}), interparticle distances, and orientations with a focus on the effect of symmetry breaking via an angle on plasmon coupling. For the model systems, the angle (θ) between the particles is varied between 0 and 180°, where θ = 0° and θ = 180° correspond to symmetric side-by-side and end-to-end orientations of the nanorods, respectively. Our analysis reveals that for a sufficiently large interparticle distance (r > 0.7 nm), where the wave-function overlap between monomers is negligible, TDDFT results agree quite well with the predictions of the dipole−dipole interaction model for the intensity of the different modes of coupled plasmons. For smaller gap distances (0.4−0.5 nm), a charge-transfer plasmon (CTP) mode occurs for the symmetry broken case of the Ag_{10} dimer. For the assemblies of larger nanorods, however, the CTP mode is predicted to be less pronounced, especially for the cases where the deviation from the end-to-end geometry is larger than 30°. The orbital overlap and configuration−interaction analyses show that these results are related to the fact that the relative overlap strength between monomeric energy levels is significantly reduced for symmetry-broken orientations of larger nanorods.

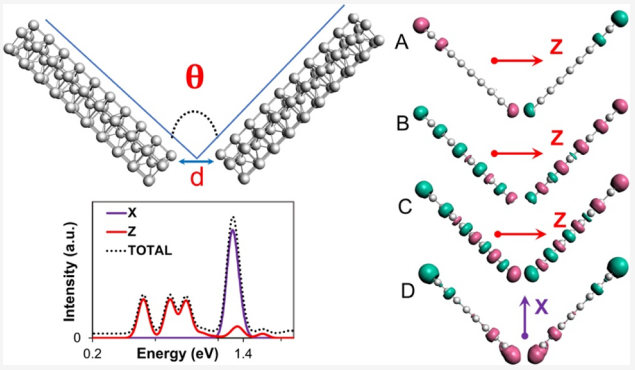

INTRODUCTION

As a result of their surface plasmon resonance (SPR),[1] metal nanoparticles show unique optical properties,[1−4] which can be controlled with the nanoparticle size, shape, and assembly geometry, or the dielectric properties of the environment.[5−7] Due to this tunability, such nanoparticles offer many potential applications in areas such as optoelectronic devices,[8,9] catalysis, or biological sensing.[10−12] For a nanoparticle dimer, the optical response and the electric-field enhancement of the system resulting from SPR can be altered compared to the case of a single nanoparticle as a result of plasmon coupling.[13−16] For large separation distances, plasmon coupling can be described by the plasmon hybridization model;[17−19] however, as the separation distances reduce to the subnanometer region, quantum-mechanical interactions between two particles need to be considered for a full description of plasmon coupling.

Theoretical treatments of plasmon coupling involve a wide array of methods[20] such as classical approaches based on solving Maxwell equations,[14,21,22] quantum-corrected methods,[23,24] or quantum-mechanical methods based on the Jellium model.[25−29] In most cases, classical approaches are sufficient to describe the plasmon coupling for a dimer system.[14,30−32] However, electron spill-out and quantum-tunneling effects become important for the optical response of the assemblies when the particle separation distance is less than 1 nm.[27,28,33,34] More recently, fully atomistic time-dependent density functional theory (TDDFT)[35−38] and approximate TDDFT methods[39−44] have been employed for the optical properties of dimer systems. In general, TDDFT-based methods suffer from high computational cost compared to classical methods and cannot be employed efficiently to nanoparticle sizes with thousands of atoms. Nevertheless, calculations on model dimer systems such as pentagonal nanorods[37,40] or icosahedral nanoparticles[42] have shown to provide important aspects of plasmon coupling from a fully quantum-mechanical standpoint.

In general, theoretical efforts on plasmon coupling have focused on the homodimers with the maximum available symmetry for the system of interest.[16,20,28] In comparison, fewer studies exist in the literature on the symmetry breaking effects on plasmon coupling.[41,45−49] It should be noted that experimentally obtained assemblies generally show a distribution of the particle size and orientation, which affects the resulting optical response of the system.[45,46] Moreover, symmetry breaking can result in new plasmon modes, which are normally dark in the perfectly

Received: March 25, 2021
Revised: May 10, 2021
Published: May 26, 2021

https://doi.org/10.1021/acs.jpcc.1c02707
J. Phys. Chem. C 2021, 125, 12198−12206

symmetric case. In an example with gold nanorod dimers, Shao et al.[50] have shown that the intensity of different modes arising from plasmon coupling strongly depend on the angle between nanorod dimers, which agrees with the theoretical predictions obtained from classical electrodynamic calculations based on the dipole−dipole interaction. These findings have also been supported in other experimental and theoretical studies, showing that the classical electrodynamics can sufficiently describe the symmetry breaking effects on plasmon coupling in such systems.[45,47−51] However, the symmetry breaking phenomena have not been explored in the quantum regime, and it is not clear whether the predictions based on the classical models will be valid for dimer assemblies with subnanometer gap distances.

In this contribution, we have systematically investigated the optical response of nanorod assemblies of different sizes using atomistic TDDFT calculations, where the angle (θ) between two particles was varied between 0 and 180° to investigate the symmetry-breaking effect on plasmon coupling via an angle. The results from the symmetry broken assemblies were compared to those obtained for the perfectly symmetric cases to understand the effect of orientation in the quantum regime. These results were also compared to the predictions of the dipole−dipole interaction model.

METHODS

All calculations were performed using the ADF2020 package.[52−54] As model systems, we have used the Ag_{10} nanowire and Ag_{59} and Ag_{139} pentagonal nanorod structures. The geometries of the monomers were optimized using the Perdew−Burke−Ernzerhof (PBE)[55] functional and a double-zeta (DZ) basis set. The assemblies were formed using the optimized geometries of monomers without further optimization. The analyzed systems included side-by-side (dimer A), end-to-end (dimer B), and symmetry broken assemblies with an angle (θ) between nanorods (dimer θ). The symmetry point group of the Ag_{10} nanowire is $D_{\infty h}$, whereas it is D_{5h} for Ag_{59} and Ag_{139}. For all systems, dimer B possesses the same symmetry as the monomers, whereas dimer A and dimer θ exhibit D_{2h} and C_{2v} symmetries, respectively. The geometries of the model systems are illustrated in Figure 1. Coordinates of the selected systems are given in the Supporting Information.

Excited states of all systems were calculated using the standard linear-response TDDFT formalism as implemented in ADF with the PBE/DZ level of theory. The optical spectra were produced from calculated excited states using a 0.15 eV full-width-half-maximum Gaussian broadening. For molecular orbital and configuration-interaction analyses, the orbitals of the monomers were labeled $nm_{g/u}$, where n (=1,2,3...) and m (=σ, π, δ,...), respectively, designate the principal quantum number and azimuthal quantum number in a cylindrical symmetry and g and u show the inversion symmetry.[37] For dimer systems, orbitals are labeled $nM_{b/a}$, where n is the same as the monomer orbitals and M is designated using capital Greek letters to differentiate the monomer and dimer levels. In this case, b and a indicate whether the dimer orbital has a bonding or an antibonding interaction between monomeric levels, respectively. A gap distance of 0.7 nm is chosen for all dimers to investigate the plasmon coupling in the lack of a significant wave-function overlap as suggested in our previous work.[37] For the quantum regime, 0.4 nm is chosen for Ag_{10} nanowires, whereas 0.45 nm is chosen for Ag_{59} and Ag_{139}. For the latter, it is seen that 0.4 nm gap distance can alter the electronic structure of dimer A significantly as a result of the strong covalent interaction, which results in problematic self-consistent field convergence. In order to view the molecular orbitals and transition-fit densities (TFDs), contour values of 0.3 and 0.00003 are used, respectively.

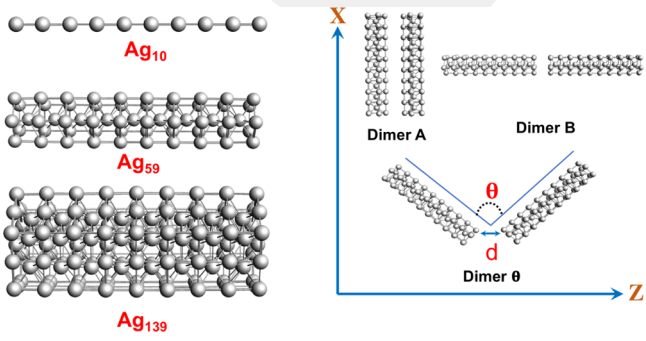

Figure 1. Geometries and orientations of the monomer and dimer model systems investigated in this study.

RESULTS AND DISCUSSION

Ag_{10} Nanowire Assemblies. In the case of the nanowire assemblies, it has been shown previously that the plasmonic peak arises from the transitions between bonding and antibonding combinations of occupied $n\sigma_{g,u}$ and unoccupied $(n + 1)\sigma_{u,g}$ levels.[37] In Figure 2a,b, we summarize the governing selection rules for the transitions in different orientations of dimer assemblies. For dimer A, only $4\Sigma_a \rightarrow 5\Sigma_a$ and $4\Sigma_b \rightarrow 5\Sigma_b$ configurations are symmetry allowed, which results in polarization along the x-axis (transverse mode), whereas $4\Sigma_b \rightarrow 5\Sigma_a$ and $4\Sigma_a \rightarrow 5\Sigma_b$ transitions are symmetry forbidden (Figure 2a). In comparison, the opposite case is true for dimer B where the resulting polarization is along the z-axis (longitudinal mode), for the nanowire assemblies with an angle (Figure 2b), all these transitions become allowed as a result of the reduced symmetry, which results in polarization across both x- and z-axes. It should be noted that a similar interaction picture can be obtained using the plasmon hybridization model for nanorod assemblies, as shown in Figure 2c,d, and in previous studies.[13,18,19] A more detailed interaction picture for the plasmon hybridization is given in Figure S1. For dimer A, only the repulsive interaction of plasmon dipoles is additive and allowed, as shown in Figure 2c, while the attractive orientation is forbidden for this geometry. For dimer B, the opposite is true as the attractive orientation of dipoles is additive and the repulsive orientation cancels each contribution completely. On the other hand, both repulsive and attractive orientations of dipoles are symmetry allowed for dimer θ (Figure 2d), where the repulsive interaction results in the transverse mode (polarized in the x direction) and attractive interaction results in the longitudinal mode (polarized in the z direction) for coupled plasmons.

In Figure 3a, we show the calculated spectra for nanowire dimers with varying angles θ at a 0.7 nm separation distance. At this distance, our previous work has shown that the wave-function overlap between monomeric levels is negligible.[37] In the case of dimer A, the spectra exhibit a single peak that blue-shifts compared to the peak in the monomeric system, as expected from the plasmon hybridization model. This peak corresponds to the transverse mode along the x-axis for coupled plasmons. As the angle changes from 0 to 30°, the peak for the transverse mode shows a considerable red shift as the repulsive

https://doi.org/10.1021/acs.jpcc.1c02707
J. Phys. Chem. C 2021, 125, 12198−12206

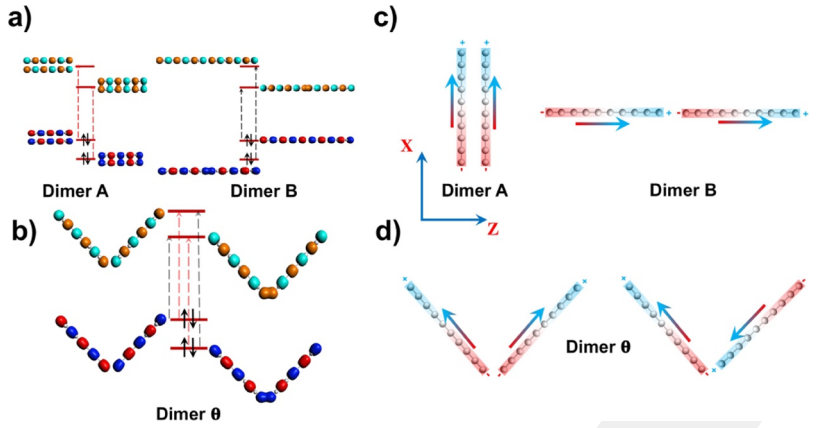

Figure 2. (a) The interaction picture and the allowed transitions for symmetric dimer A and dimer B assemblies. (b) The same interaction picture for the symmetry-broken (dimer θ) assemblies. For dimer A, only bonding → bonding and antibonding → antibonding transitions (vertical arrows) are allowed, whereas only bonding → antibonding and antibonding → bonding transitions are allowed for dimer B due to the symmetry of these assemblies. (c) Dipole-allowed modes for the coupled plasmons in the case of symmetric assemblies and (d) dipole-allowed modes in the case of symmetry-broken (dimer θ) assemblies.

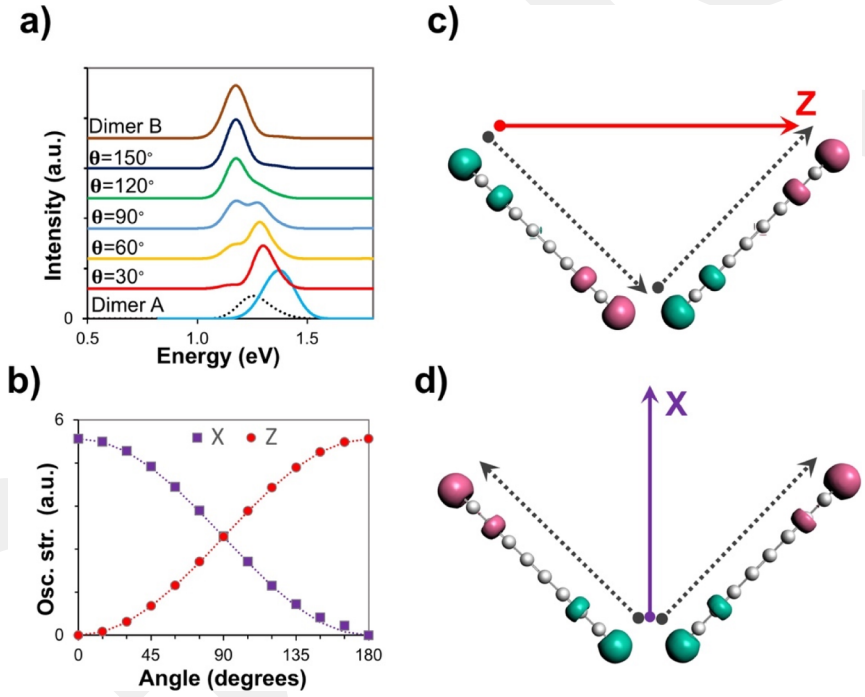

Figure 3. (a) Calculated spectra for Ag_{10} assemblies for varying angles between nanowires with a 0.7 nm gap distance. Black dotted curve shows the monomer spectrum. (b) Comparison of the total oscillator strengths (osc. str.) for transverse (X) and longitudinal (Z) modes. The dotted lines represent the $A\cos^2(\theta/2)$ and $B\sin^2(\theta/2)$ curves for X and Z directions, respectively. (c) TFD of the longitudinal mode for dimer 90° and (d) TFD for the transverse mode for the same orientation.

interaction between two dipoles is expected to be the largest in the case of dimer A. In addition, the longitudinal mode, which is red-shifted compared to the monomeric case, is predicted for this assembly as a small feature in the spectra. As the angle between nanowires increases, the red-shifted peak gradually gains intensity, whereas the intensity of the blue-shifted peak becomes smaller. When $\theta = 90°$, the intensities of the peaks are quite similar as expected from the classical vector-addition model of the dipole moments, as summarized in Figure S2. For this angle, calculated TFDs also show a good agreement with the classical dipole model, as illustrated in Figure 3c,d, for the longitudinal and transverse modes, respectively. For these modes, plasmon coupling exhibits the bonding dipole plasmon (BDP) interaction as described by the plasmon hybridization model. When θ is between 90 and 180°, the longitudinal mode gradually becomes more intense compared to the transverse mode and finally becomes the single feature for the given energy range for the dimer B geometry.

As seen from the TFDs and the calculated spectra, the broken symmetry in nanorod assemblies at 0.7 nm separation distance behaves quite similarly to what would be expected from a plasmon hybridization model. This agreement between the two approaches can also be seen in Figure 3b, where we compare the total oscillator strengths of longitudinal and transverse modes with respect to varying θ. The calculated energies and oscillator strengths of these excited states are given in Table S1. It is seen

https://doi.org/10.1021/acs.jpcc.1c02707
J. Phys. Chem. C 2021, 125, 12198−12206

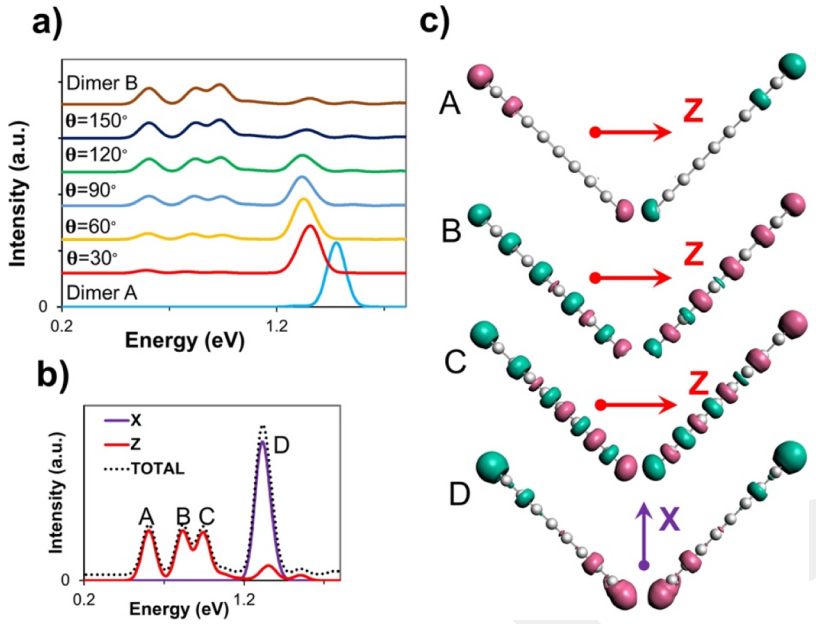

Figure 4. (a) Calculated spectra for Ag_{10} assemblies with varying angles between nanowires at 0.4 nm gap distance, (b) polarization-dependent spectra of dimer 90°, (c) TFDs of different longitudinal modes (A, B, and C), and transverse mode (D) for dimer 90° with 0.4 nm gap distance.

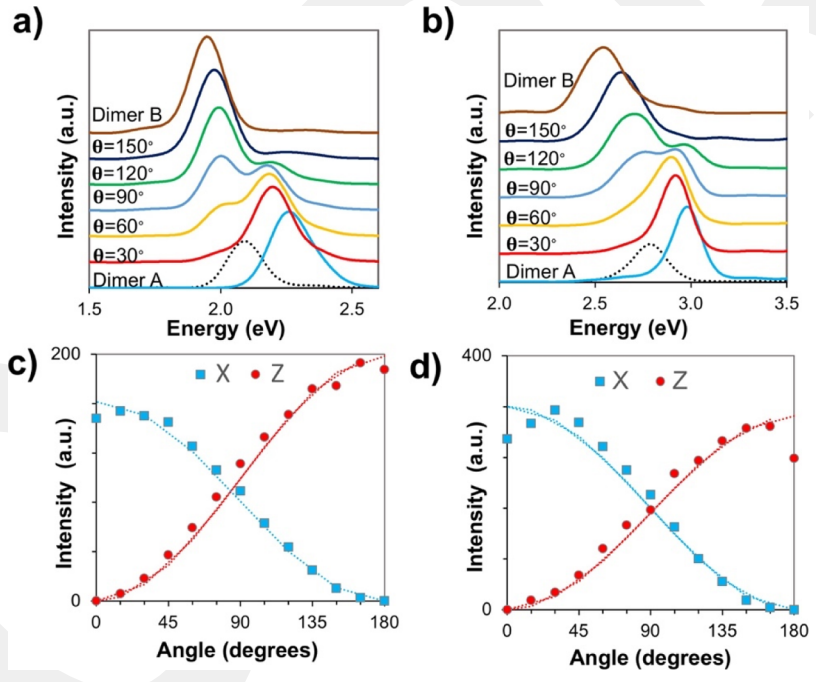

Figure 5. Calculated spectra for (a) Ag_{59} and (b) Ag_{139} assemblies for varying angles at 0.7 nm gap distance (black dotted curves show the monomer spectra), and comparison of the intensities for transverse (X) and longitudinal (Z) modes for (c) Ag_{59} and (d) Ag_{139} assemblies. The dotted lines represent the $A \sin^2(\theta/2)$ and $B \cos^2(\theta/2)$ curves.

that the variation in the oscillator strength can be fitted to the $A \sin^2(\theta/2)$ and $B \cos^2(\theta/2)$ curves for the longitudinal peaks in the z and x directions, respectively. This dependence can also be realized by applying the law of cosines to the addition of transition-dipole moments (Figure S2) of the different modes, as shown in Figure 2b. These results demonstrate that classical and quantum models can both describe the plasmon coupling for symmetry-broken orientations in nanowires when the gap distance is sufficiently large such that wave-function overlaps between monomeric levels are negligible.

At this point, we turn our attention to smaller gap distances where charge-transfer plasmons (CTPs) are predicted previously for nanowires in the dimer B assembly.[37] In Figure 4a, we show the calculated spectra for nanowire assemblies at a 0.4 nm gap distance with varying θ. At this distance, the covalent interaction between monomeric wave functions is considerably large, which is shown to be essential for the emergence of the CTP mode. In the case of the dimer A assembly, a single feature is predicted again, similar to the 0.7 nm gap distance for the longitudinal peak in the x direction. As expected, the intensity of this peak becomes smaller with increasing θ. For the z direction,

https://doi.org/10.1021/acs.jpcc.1c02707
J. Phys. Chem. C 2021, 125, 12198−12206

however, new features arise in the spectra as θ deviates from 0°. All these features systematically gain intensity as θ increase.

In Figure 4b, we show the polarization-dependent spectra for the $\theta = 90°$ case along with the overall spectrum, whereas Figure 4c illustrates the TFDs for these features. It is clear that the splitting of the plasmon only occurs for the longitudinal mode, whereas the transverse mode remains as a single feature. Additionally, the TFD of the transverse mode (D) shows a BDP mode similar to the case in the 0.7 nm gap distance. On the other hand, TFDs of the longitudinal modes clearly show a CTP character for peaks A and B and a distorted BDP character for peak C. Interestingly, the energy spacings, relative intensities, and TFDs of these new features are very similar in assemblies with the broken symmetry when compared to the case in dimer B. This is also evident from the comparison of excited-state configurations and oscillator strengths for different assemblies, as shown in Table S2. It should also be noted that the splitting of CTP and BDP modes in dimer B assemblies are shown to be most pronounced when GGA functionals are employed, and the intensities and energy separation of these modes depend on the percentage of Hartree−Fock exchange in the functional.[37] We expect a similar dependence with the choice of the functional for the symmetry-broken assemblies as well. In comparison, experimental evidence for different assemblies of nanoparticles suggest the formation of CTP for gap distances less than 1 nm,[33,56,57] which shows a qualitative agreement with the results obtained with GGA functionals.

Ag_{59} and Ag_{139} Nanorod Assemblies. In this section, we turn our attention to model nanorod systems with a larger width to investigate the size evolution of the plasmon coupling in broken-symmetry assemblies. We note that the interaction picture for larger nanorods is quite similar to the case in nanowires, as shown in Figure 2, except for the fact that configurations with higher azimuthal quantum numbers such as $\Pi \rightarrow \Pi$ or $\Delta \rightarrow \Delta$ also participate for the plasmon modes. In Figure 5a,b, we show the calculated spectra for Ag_{59} and Ag_{139} nanorod assemblies, respectively, with a 0.7 nm gap distance. For both systems, the effects in the calculated spectra from changing θ show a strong resemblance to the case of nanowires. As seen from Figure 5c,d, the calculated intensities of the peaks follow a similar $\sin^2(\theta/2)$ or $\cos^2(\theta/2)$ dependence, especially for the cases when the θ is between 30 and 150°. However, when the nanorods are close to being perfectly aligned on the x- (dimer A) or z axis (dimer B), there is some broadening effects for the plasmon peak, and the calculated intensities deviate from the expected dipole-model dependence. This deviation becomes larger with the increasing nanorod size as seen from the comparison between Ag_{59} and Ag_{139} nanorod assemblies.

In addition to the calculated intensities, there are differences in the calculated energy shift of the longitudinal peak with respect to the aspect ratio of the model systems as the symmetry of the assembly deviates slightly from the dimer A or dimer B geometry. As mentioned earlier, the energy of the plasmon mode in the z direction shows little dependence on θ for the Ag_{10} nanowire assemblies, whereas the plasmon mode in the x direction shows a ∼0.1 eV red shift as θ changes from 0° (dimer A geometry) to 30°. For the same angle change, both Ag_{59} and Ag_{139} assemblies exhibit a similar red shift for the transverse (x direction) mode. In comparison, the blue shift for the longitudinal mode depends on the width of the nanorod. While there is no noticeable energy change for Ag_{10} nanowire assemblies, there is a small but noticeable blue shift for the longitudinal mode in the case of Ag_{59} (∼0.05 eV) as θ changes from 180 to 150°. For the same angle change, this blue shift becomes ∼0.25 eV for Ag_{139} nanorod assemblies. This is mainly related to the fact that the attractive or repulsive Coulomb interaction between transition dipoles of the plasmon modes is maximized when the nanorods are aligned in the z or x direction. As the width of the nanorods increases, the difference in the magnitude of this interaction becomes significant for the longitudinal mode even for a small deviation from the dimer B case.

Except for the magnitude of the energy shift and the broadening effects for plasmon modes, there is a good agreement between different nanorod models for the overall shape of the spectrum as well as with the predictions of the classical dipole model when the distance between monomers is ∼0.7 nm or larger. However, this is not the case for smaller gaps where there is a potential orbital interaction between monomeric levels. In Figure 6, we show the θ dependence of

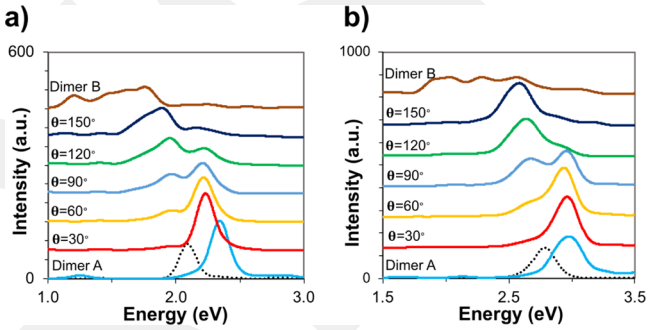

Figure 6. Calculated spectra for (a) Ag_{59} and (b) Ag_{139} assemblies for varying angles at 0.45 nm gap distance.

the calculated spectra for Ag_{59} and Ag_{139} nanorod assemblies for a gap distance of 0.45 nm. For both cases, the dimer A geometry exhibits a blue-shifted single peak for the transverse mode as expected. In comparison, dimer B spectra exhibit significant splitting for the longitudinal plasmon due to the formation of low-energy CTP modes similar to the case of the Ag_{10} assemblies (Figure 3) and in previous studies with similar nanorod systems.[37,38,40] As mentioned earlier, the formation of the CTP mode along with the splitting of different plasmon modes is also observed for broken-symmetry assemblies ($\theta \neq 0°$ or $\theta \neq 180°$) in the case of the Ag_{10} nanowire. For Ag_{59} and Ag_{139} nanorods, however, this splitting is much less pronounced, as shown in Figure 6. In the case of Ag_{59} assemblies, the longitudinal mode mainly shows an asymmetric, broad feature around 2.0 eV, with additional small-intensity features in the low-energy region (1.0−1.5 eV). Unlike Ag_{10} dimers, the spectral shape and energetics of the peaks become significantly different as θ changes from 180 to 150°. This is also the case for Ag_{139} assemblies. In fact, except for the dimer B orientation, the evolution of the spectra is surprisingly similar to the case where the gap distance is 0.7 nm, and the formation of CTP modes is not predicted for symmetry-broken assemblies of the Ag_{139} nanorod.

To further understand the size evolution of the plasmon coupling for small-gap distances, we investigate the role of the orbital interaction for our model systems. In our previous work with dimer B assemblies,[37] it was shown that the formation of the CTP mode mainly results when there is significant energy and dipole moment contribution difference for the transitions involving bonding and antibonding combinations of monomeric

https://doi.org/10.1021/acs.jpcc.1c02707
J. Phys. Chem. C 2021, 125, 12198−12206

orbitals, as shown in Figure 3b. For such transitions, it was found from a configuration−interaction standpoint that the constructive coupling of these transitions results in the BDP mode, whereas the destructive coupling results in the CTP mode. Of course, such a difference only occurs when there is a significant overlap between monomeric levels. In Table 1, we show the

Table 1. Occupied−Unoccupied Energy Differences (ΔE) and Oscillator Strengths of Selected Single Configurations for Different Orientations of Nanorods for a 0.45 nm Gap Distance

	θ = 0° (dimer A)		θ = 180° (dimer B)		θ = 90°	
transitions	ΔE (eV)	oscillator strength (a.u.)	ΔE (eV)	oscillator strength (a.u.)	ΔE (eV)	oscillator strength (a.u.)
Ag_{10} Nanowire						
$5^b\Sigma \rightarrow 6^b\Sigma$	0.48	2.96	0.46	0.00[b]	0.47	1.44
$5^a\Sigma \rightarrow 6^a\Sigma$	0.47	2.94	0.50	0.00[b]	0.49	1.50
$5^b\Sigma \rightarrow 6^a\Sigma$	0.87	0.00[a]	0.57	1.54	0.57	0.71
$5^a\Sigma \rightarrow 6^b\Sigma$	0.09	0.00[a]	0.39	4.48	0.40	2.36
Ag_{59} Nanorod						
$7^b\Pi \rightarrow 8^b\Pi$	0.66	9.08	0.66	0.00[b]	0.67	4.13
$7^a\Pi \rightarrow 8^a\Pi$	0.68	9.10	0.69	0.00[b]	0.68	4.30
$7^b\Pi \rightarrow 8^a\Pi$	0.74	0.00[a]	0.78	5.20	0.70	3.97
$7^a\Pi \rightarrow 8^b\Pi$	0.63	0.00[a]	0.57	13.44	0.65	5.08
Ag_{139} Nanorod						
$7^b\Delta \rightarrow 8^b\Delta$	0.81	9.15	0.80	0.00[b]	0.81	4.45
$7^a\Delta \rightarrow 8^a\Delta$	0.81	8.19	0.84	0.00[b]	0.81	4.23
$7^b\Delta \rightarrow 8^a\Delta$	0.84	0.00[a]	0.92	6.35	0.83	4.38
$7^a\Delta \rightarrow 8^b\Delta$	0.79	0.00[a]	0.71	13.14	0.80	5.41

[a]The bonding → antibonding or antibonding → bonding transitions are dipole-forbidden due to the symmetry for the dimer A orientation. [b]The bonding → bonding or antibonding → antibonding transitions are dipole-forbidden due to the symmetry for the dimer B orientation.

energies and oscillator strengths of the single transitions with the largest dipole moment contributions to the plasmonic peak for each model system where the gap distance is 0.45 nm. For all systems, the transverse mode mainly emerges as a single peak for different gap distances and symmetry. As shown in Table 1, allowed transitions for this mode are bonding → bonding and antibonding → antibonding in nature due to the symmetry. As a result, these configurations exhibit similar transition energies and oscillator strengths for all systems. In comparison, allowed transitions for the longitudinal modes are bonding → antibonding and antibonding → bonding types, and these transition pairs show significant differences for their oscillator strengths and energies when there is an orbital overlap between monomeric levels. For the dimer B assemblies of Ag_{10}, Ag_{59}, and Ag_{139}, the ratios of the oscillator strengths for these transitions are 0.34, 0.38, and 0.48, whereas the energy differences are 0.18, 0.21, and 0.21 eV, respectively. We note that for gap distance such as 0.7 nm, the oscillator strength ratio and energy difference between these configurations are essentially 1.00 and 0.00, respectively, due to the lack of orbital interaction between monomeric levels.

For the assemblies with a broken symmetry (θ = 90°), the oscillator strength and energy difference between bonding → antibonding and antibonding → bonding type transitions show a clear size dependence. In the case of the $\Sigma \rightarrow \Sigma$ transitions of Ag_{10} assemblies, the energy difference and oscillator strength ratio are 0.17 eV and 0.30, respectively, indicating that the orbital interaction does not change significantly with θ for this model. As a result, the splitting pattern of the plasmon mode in the z direction is quite similar between different orientations except for the intensity of the peaks, as shown in Figure 4. On the other hand, the energy difference and oscillator strength ratio of $\Pi \rightarrow \Pi$ transitions for Ag_{59} are 0.05 eV and 0.78, indicating a significant reduction for the coupling of monomeric orbitals from θ = 180° to θ = 90°. Similarly, the same energy difference and oscillator strength ratio become 0.03 eV and 0.81 for the $\Delta \rightarrow \Delta$ transition of the dimer 90 assembly of the Ag_{139} nanorod. These results are further illustrated from an orbital interaction standpoint, as shown in Figure 7. For Ag_{10}, the total overlap

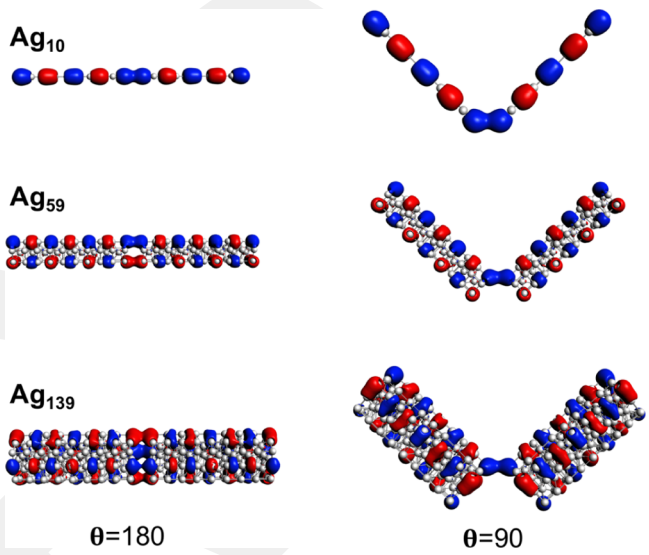

Figure 7. Illustration of the orbital overlap (bonding interaction) for $\Sigma \rightarrow \Sigma$ transitions of Ag_{10}, $\Pi \rightarrow \Pi$ transitions for Ag_{59}, and $\Delta \rightarrow \Delta$ transitions of Ag_{139} in dimer B and dimer 90° assemblies.

between monomeric levels does not change from dimer B to dimer 90 assemblies because the overlap mainly occurs over two atoms. As the aspect ratio of the nanorod increases, the net overlap between monomeric levels decreases. Moreover, with the increasing aspect ratio, configurations with higher azimuthal quantum numbers become important for the plasmonic peak, and the effect of symmetry breaking can become even more drastic. As a result, splitting of the plasmonic peak is less likely for larger nanorods as the orientation of the dimer deviates from dimer B.

Finally, we investigate the Ag_{139} assemblies where θ is within the range of 180−150° to understand whether plasmon splitting occurs for these orientations. In Figure 8a, the calculated spectra are shown for these geometries, while Figure 8b,c shows the oscillator strength ratio and energy difference between $7\Delta_b \rightarrow 8\Delta_a$ and $7\Delta_a \rightarrow 8\Delta_b$ configurations, respectively. As seen from the spectra, there are only minor changes for the splitting of the plasmon mode when the deviation from the dimer B geometry is only 5° (θ = 175°). This is also evident from the oscillator strength ratio and the energy difference of the configurations, which indicate that the orbital overlap between monomeric levels is not altered significantly for this orientation compared to the dimer B case. However, with increasing deviation from the dimer B geometry, the coupling between monomeric levels is decreased significantly, and the oscillator strength ratio and energy difference between $7\Delta_b \rightarrow 8\Delta_a$ and $7\Delta_a \rightarrow 8\Delta_b$ configurations approach to the case where θ = 90°. As a result,

https://doi.org/10.1021/acs.jpcc.1c02707
J. Phys. Chem. C 2021, 125, 12198−12206

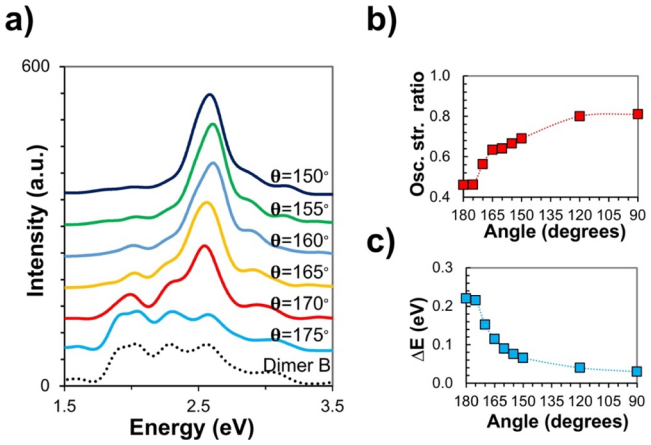

Figure 8. (a) Calculated spectra for Ag_{139} assemblies for orientation angles between 150 and 180° at 0.45 nm gap distance, (b) oscillator strength ratio, and (c) energy difference between $7\Delta_b \rightarrow 8\Delta_a$ and $7\Delta_a \rightarrow 8\Delta_b$ configurations for these geometries.

the low-energy plasmon modes in the spectra become gradually smaller in intensity, and a single feature is mainly predicted for the plasmon mode in the z direction for deviations larger than 30°. Our results show that for nanorods with a small aspect ratio and large width, the formation of the CTP mode is possible for slight deviations from the perfectly aligned geometry; however, the spectra mainly show a single mode when this deviation is larger than 30° due to the reduced interaction between monomeric orbitals.

CONCLUSIONS

In summary, we have performed an atomistic TDDFT investigation of the plasmon coupling in dimer assemblies of Ag_{10}, Ag_{59}, and Ag_{139} nanorods with varying angles. For gap distances such as 0.7 nm where no significant overlap between monomeric levels occurs, the coupling of the plasmon modes agrees well with the predictions of the dipole model. For these assemblies, the intensities of the longitudinal and transverse modes generally follow $\sin^2(\theta/2)$ or $\cos^2(\theta/2)$ dependences, respectively, with respect to the varying angles between nanorods. However, when two nanorods are close to being perfectly aligned, some broadening effects occur for the plasmonic peak and the calculated intensities become smaller compared to the predictions of the dipole model.

For small gap distances (0.4−0.5 nm), where there is a significant orbital overlap between monomeric levels, the formation of CTP modes is observed in the case of symmetry-broken assemblies of Ag_{10} dimers. Additionally, the energy spacing and the relative intensities of different modes are quite similar for perfectly aligned (dimer B) and symmetry-broken dimers. For nanorods with a larger width (Ag_{59} and Ag_{139}), however, the splitting of the plasmonic peak is found to be much less pronounced for symmetry-broken assemblies. For these systems, different plasmon modes are formed with only small deviations from the dimer B geometry, whereas only a single peak is predicted for Ag_{139} assemblies when the deviation from the dimer B geometry is more than 30°. Configuration interaction and orbital analyses have revealed that these results are related to the fact that the relative overlap strength between monomer levels is reduced significantly for symmetry-broken orientations of large nanorods.

ASSOCIATED CONTENT

Supporting Information

The Supporting Information is available free of charge at https://pubs.acs.org/doi/10.1021/acs.jpcc.1c02707.

Summary of the plasmon hybridization model for the plasmon coupling; energies, and oscillator strengths of the transitions in Ag_{10} dimers with gap distances of 0.7 nm and 0.4 nm; illustration of the dipole model for selective clusters investigated in this work and XYZ coordinates for selective dimers (PDF)

AUTHOR INFORMATION

Corresponding Authors

Fahri Alkan − *Department of Nanotechnology Engineering, Abdullah Gül University, Kayseri 38080, Turkey;* orcid.org/0000-0002-4046-9044; Email: fahri.alkan@agu.edu.tr

Christine M. Aikens − *Department of Chemistry, Kansas State University, Manhattan, Kansas 66506, United States;* orcid.org/0000-0002-0854-7997; Email: cmaikens@ksu.edu

Complete contact information is available at: https://pubs.acs.org/10.1021/acs.jpcc.1c02707

Notes

The authors declare no competing financial interest.

ACKNOWLEDGMENTS

The computing for this project was performed at the HPC Center at Abdullah Gül University. This material is based on the work supported by the Air Force Office of Scientific Research under Grant no. F9550-15-0114.

REFERENCES

(1) Link, S.; El-Sayed, M. A. Spectral Properties and Relaxation Dynamics of Surface Plasmon Electronic Oscillations in Gold and Silver Nanodots and Nanorods. *J. Phys. Chem. B* **1999**, *103*, 8410−8426.

(2) Yu, Y. Y.; Chang, S.-S.; Lee, C.-L.; Wang, C. R. C. Gold Nanorods: Electrochemical Synthesis and Optical Properties. *J. Phys. Chem. B* **1997**, *101*, 6661−6664.

(3) Eustis, S.; El-Sayed, M. A. Why Gold Nanoparticles Are More Precious Than Pretty Gold: Noble Metal Surface Plasmon Resonance and Its Enhancement of the Radiative and Nonradiative Properties of Nanocrystals of Different Shapes. *Chem. Soc. Rev.* **2006**, *35*, 209−217.

(4) Wang, H.; Brandl, D. W.; Nordlander, P.; Halas, N. J. Plasmonic Nanostructures: Artificial Molecules. *Acc. Chem. Res.* **2007**, *40*, 53−62.

(5) Kelly, K. L.; Coronado, E.; Zhao, L. L.; Schatz, G. C. The Optical Properties of Metal Nanoparticles: The Influence of Size, Shape, and Dielectric Environment. *J. Phys. Chem. B* **2003**, *107*, 668−677.

(6) Jain, P. K.; Lee, K. S.; El-Sayed, I. H.; El-Sayed, M. A. Calculated Absorption and Scattering Properties of Gold Nanoparticles of Different Size, Shape, and Composition: Applications in Biological Imaging and Biomedicine. *J. Phys. Chem. B* **2006**, *110*, 7238−7248.

(7) Ma, Y.; Li, W.; Cho, E. C.; Li, Z.; Yu, T.; Zeng, J.; Xie, Z.; Xia, Y. Au@Ag Core−Shell Nanocubes with Finely Tuned and Well-Controlled Sizes, Shell Thicknesses, and Optical Properties. *ACS Nano* **2010**, *4*, 6725−6734.

(8) Chen, Y. S.; Choi, H.; Kamat, P. V. Metal-Cluster-Sensitized Solar Cells. A New Class of Thiolated Gold Sensitizers Delivering Efficiency Greater Than 2%. *J. Am. Chem. Soc.* **2013**, *135*, 8822−8825.

(9) Zhang, Y.; Chu, W.; Foroushani, A.; Wang, H.; Li, D.; Liu, J.; Barrow, C.; Wang, X.; Yang, W. New Gold Nanostructures for Sensor Applications: A Review. *Materials* **2014**, *7*, 5169−5201.

(10) El-Sayed, I. H.; Huang, X.; El-Sayed, M. A. Surface Plasmon Resonance Scattering and Absorption of Anti-EGFR Antibody Conjugated Gold Nanoparticles in Cancer Diagnostics: Applications in Oral Cancer. *Nano Lett.* **2005**, *5*, 829−834.
(11) Yang, X.; Yang, M.; Pang, B.; Vara, M.; Xia, Y. Gold Nanomaterials at Work in Biomedicine. *Chem. Rev.* **2015**, *115*, 10410−10488.
(12) Vigderman, L.; Khanal, B. P.; Zubarev, E. R. Functional Gold Nanorods: Synthesis, Self-Assembly, and Sensing Applications. *Adv. Mater.* **2012**, *24*, 4811−4841.
(13) Halas, N. J.; Lal, S.; Chang, W.-S.; Link, S.; Nordlander, P. Plasmons in Strongly Coupled Metallic Nanostructures. *Chem. Rev.* **2011**, *111*, 3913−3961.
(14) Jain, P. K.; Eustis, S.; El-Sayed, M. A. Plasmon Coupling in Nanorod Assemblies: Optical Absorption, Discrete Dipole Approximation Simulation, and Exciton-Coupling Model. *J. Phys. Chem. B* **2006**, *110*, 18243−18253.
(15) Tabor, C.; Murali, R.; Mahmoud, M.; El-Sayed, M. A. On the Use of Plasmonic Nanoparticle Pairs as a Plasmon Ruler: The Dependence of the near-Field Dipole Plasmon Coupling on Nanoparticle Size and Shape. *J. Phys. Chem. A* **2009**, *113*, 1946−1953.
(16) Jain, P. K.; El-Sayed, M. A. Plasmonic Coupling in Noble Metal Nanostructures. *Chem. Phys. Lett.* **2010**, *487*, 153−164.
(17) Prodan, E.; Radloff, C.; Halas, N. J.; Nordlander, P. A Hybridization Model for the Plasmon Response of Complex Nanostructures. *Science* **2003**, *302*, 419−422.
(18) Willingham, B.; Brandl, D. W.; Nordlander, P. Plasmon Hybridization in Nanorod Dimers. *Appl. Phys. B Laser Opt.* **2008**, *93*, 209−216.
(19) Nordlander, P.; Oubre, C.; Prodan, E.; Li, K.; Stockman, M. I. Plasmon Hybridization in Nanoparticle Dimers. *Nano Lett.* **2004**, *4*, 899−903.
(20) Morton, S. M.; Silverstein, D. W.; Jensen, L. Theoretical Studies of Plasmonics Using Electronic Structure Methods. *Chem. Rev.* **2011**, *111*, 3962−3994.
(21) McMahon, J. M.; Gray, S. K.; Schatz, G. C. Nonlocal Optical Response of Metal Nanostructures with Arbitrary Shape. *Phys. Rev. Lett.* **2009**, *103*, 097403.
(22) Myroshnychenko, V.; Rodríguez-Fernández, J.; Pastoriza-Santos, I.; Funston, A. M.; Novo, C.; Mulvaney, P.; Liz-Marzán, L. M.; García de Abajo, F. J. Modelling the Optical Response of Gold Nanoparticles. *Chem. Soc. Rev.* **2008**, *37*, 1792−1805.
(23) Esteban, R.; Borisov, A. G.; Nordlander, P.; Aizpurua, J. Bridging Quantum and Classical Plasmonics with a Quantum-Corrected Model. *Nat. Commun.* **2012**, *3*, 825.
(24) Teperik, T. V.; Nordlander, P.; Aizpurua, J.; Borisov, A. G. Quantum Effects and Nonlocality in Strongly Coupled Plasmonic Nanowire Dimers. *Opt. Express* **2013**, *21*, 27306−27325.
(25) Prodan, E.; Nordlander, P. Structural Tunability of the Plasmon Resonances in Metallic Nanoshells. *Nano Lett.* **2003**, *3*, 543−547.
(26) Lassiter, J. B.; Aizpurua, J.; Hernandez, L. I.; Brandl, D. W.; Romero, I.; Lal, S.; Hafner, J. H.; Nordlander, P.; Halas, N. J. Close Encounters between Two Nanoshells. *Nano Lett.* **2008**, *8*, 1212−1218.
(27) Zuloaga, J.; Prodan, E.; Nordlander, P. Quantum Description of the Plasmon Resonances of a Nanoparticle Dimer. *Nano Lett.* **2009**, *9*, 887−891.
(28) Varas, A.; García-González, P.; Feist, J.; García-Vidal, F. J.; Rubio, A. Quantum Plasmonics: From Jellium Models to Ab Initio Calculations. *Nanophotonics* **2016**, *5*, 409−426.
(29) Selenius, E.; Malola, S.; Häkkinen, H. Analysis of Localized Surface Plasmon Resonances in Spherical Jellium Clusters and Their Assemblies. *J. Phys. Chem. C* **2017**, *121*, 27036−27052.
(30) Jain, P. K.; Huang, W.; El-Sayed, M. A. On the Universal Scaling Behavior of the Distance Decay of Plasmon Coupling in Metal Nanoparticle Pairs: A Plasmon Ruler Equation. *Nano Lett.* **2007**, *7*, 2080−2088.
(31) Fofang, N. T.; Park, T.-H.; Neumann, O.; Mirin, N. A.; Nordlander, P.; Halas, N. J. Plexcitonic Nanoparticles: Plasmon−Exciton Coupling in Nanoshell−J-Aggregate Complexes. *Nano Lett.* **2008**, *8*, 3481−3487.
(32) Jain, P. K.; El-Sayed, M. A. Noble Metal Nanoparticle Pairs: Effect of Medium for Enhanced Nanosensing. *Nano Lett.* **2008**, *8*, 4347−4352.
(33) Xu, D.; Xiong, X.; Wu, L.; Ren, X.-F.; Png, C. E.; Guo, G.-C.; Gong, Q.; Xiao, Y.-F. Quantum Plasmonics: New Opportunity in Fundamental and Applied Photonics. *Adv. Opt Photon* **2018**, *10*, 703−756.
(34) Winther, K. T.; Jensen, K. L.; Mortensen, N. A.; Thygesen, K. S. Visualizing Hybridized Quantum Plasmons in Coupled Nanowires: From Classical to Tunneling Regime. *Phys. Rev. B: Condens. Matter Mater. Phys.* **2013**, *87*, 235433.
(35) Vincenot, J.; Aikens, C. M. Quantum Mechanical Examination of Optical Absorption Spectra of Silver Nanorod Dimers. In *Advances in the Theory of Atomic and Molecular Systems*; Piecuch, P., Maruani, J., Delgado-Barrio, G., Wilson, S., Eds.; Springer Netherlands, 2009; Vol. *20*, p 253−264.
(36) Bae, G.-T.; Aikens, C. M. TDDFT and CIS Studies of Optical Properties of Dimers of Silver Tetrahedra. *J. Phys. Chem. A* **2012**, *116*, 8260−8269.
(37) Alkan, F.; Aikens, C. M. Understanding Plasmon Coupling in Nanoparticle Dimers Using Molecular Orbitals and Configuration Interaction. *Phys. Chem. Chem. Phys.* **2019**, *21*, 23065−23075.
(38) Fitzgerald, J. M.; Azadi, S.; Giannini, V. Quantum Plasmonic Nanoantennas. *Phys. Rev. B* **2017**, *95*, 235414.
(39) Xiang, H.; Zhang, M.; Zhang, X.; Lu, G. Understanding Quantum Plasmonics from Time-Dependent Orbital-Free Density Functional Theory. *J. Phys. Chem. C* **2016**, *120*, 14330−14336.
(40) Alkan, F.; Aikens, C. M. TD-DFT and TD-DFTB Investigation of the Optical Properties and Electronic Structure of Silver Nanorods and Nanorod Dimers. *J. Phys. Chem. C* **2018**, *122*, 23639−23650.
(41) Liu, Z.; Alkan, F.; Aikens, C. M. TD-DFTB Study of Optical Properties of Silver Nanoparticle Homodimers and Heterodimers. *J. Chem. Phys.* **2020**, *153*, 144711.
(42) Ilawe, N. V.; Oviedo, M. B.; Wong, B. M. Real-Time Quantum Dynamics of Long-Range Electronic Excitation Transfer in Plasmonic Nanoantennas. *J. Chem. Theory Comput.* **2017**, *13*, 3442−3454.
(43) Ilawe, N. V.; Oviedo, M. B.; Wong, B. M. Effect of Quantum Tunneling on the Efficiency of Excitation Energy Transfer in Plasmonic Nanoparticle Chain Waveguides. *J. Mater. Chem. C* **2018**, *6*, 5857−5864.
(44) Fedorov, A. S.; Krasnov, P. O.; Visotin, M. A.; Tomilin, F. N.; Polyutov, S. P.; Ågren, H. Charge-Transfer Plasmons with Narrow Conductive Molecular Bridges: A Quantum-Classical Theory. *J. Chem. Phys.* **2019**, *151*, 244125.
(45) Funston, A. M.; Novo, C.; Davis, T. J.; Mulvaney, P. Plasmon Coupling of Gold Nanorods at Short Distances and in Different Geometries. *Nano Lett.* **2009**, *9*, 1651−1658.
(46) Brown, L. V.; Sobhani, H.; Lassiter, J. B.; Nordlander, P.; Halas, N. J. Heterodimers: Plasmonic Properties of Mismatched Nanoparticle Pairs. *ACS Nano* **2010**, *4*, 819−832.
(47) Panaro, S.; Nazir, A.; Liberale, C.; Das, G.; Wang, H.; De Angelis, F.; Proietti Zaccaria, R.; Di Fabrizio, E.; Toma, A. Dark to Bright Mode Conversion on Dipolar Nanoantennas: A Symmetry-Breaking Approach. *ACS Photonics* **2014**, *1*, 310−314.
(48) Wu, J.; Lu, X.; Zhu, Q.; Zhao, J.; Shen, Q.; Zhan, L.; Ni, W. Angle-Resolved Plasmonic Properties of Single Gold Nanorod Dimers. *Nano-Micro Lett.* **2014**, *6*, 372−380.
(49) Tabor, C.; Van Haute, D.; El-Sayed, M. A. Effect of Orientation on Plasmonic Coupling between Gold Nanorods. *ACS Nano* **2009**, *3*, 3670−3678.
(50) Shao, L.; Woo, K. C.; Chen, H.; Jin, Z.; Wang, J.; Lin, H.-Q. Angle- and Energy-Resolved Plasmon Coupling in Gold Nanorod Dimers. *ACS Nano* **2010**, *4*, 3053−3062.
(51) Slaughter, L. S.; Wu, Y.; Willingham, B. A.; Nordlander, P.; Link, S. Effects of Symmetry Breaking and Conductive Contact on the Plasmon Coupling in Gold Nanorod Dimers. *ACS Nano* **2010**, *4*, 4657−4666.

https://doi.org/10.1021/acs.jpcc.1c02707
J. Phys. Chem. C 2021, 125, 12198−12206

(52) ADF2020 SCM. *Theoretical Chemistry*; Vrije Universities: Amsterdam, The Netherlands, http://www.scm.com, accessed 12/20/2019.
(53) Guerra, C. F.; Snijders, J. G.; te Velde, G.; Baerends, E. J. Towards an Order-N DFT Method. *Theor. Chem. Acc.* **1998**, *99*, 391−403.
(54) te Velde, G.; Bickelhaupt, F. M.; Baerends, E. J.; Fonseca Guerra, C.; Van Gisbergen, S. J. A.; Snijders, J. G.; Ziegler, T. Chemistry with Adf. *J. Comput. Chem.* **2001**, *22*, 931−967.
(55) Perdew, J. P.; Burke, K.; Ernzerhof, M. Generalized Gradient Approximation Made Simple. *Phys. Rev. Lett.* **1996**, *77*, 3865−3868.
(56) Savage, K. J.; Hawkeye, M. M.; Esteban, R.; Borisov, A. G.; Aizpurua, J.; Baumberg, J. J. Revealing the Quantum Regime in Tunnelling Plasmonics. *Nature* **2012**, *491*, 574−577.
(57) Tan, S. F.; Wu, L.; Yang, J. K. W.; Bai, P.; Bosman, M.; Nijhuis, C. A. Quantum Plasmon Resonances Controlled by Molecular Tunnel Junctions. *Science* **2014**, *343*, 1496−1499.

https://doi.org/10.1021/acs.jpcc.1c02707
J. Phys. Chem. C 2021, 125, 12198−12206